Ionospheric response to earthquakes of different magnitudes: Larger quakes perturb the ionosphere stronger and longer

E. Astafyeva,[1] S. Shalimov,[2,3] E. Olshanskaya,[2] and P. Lognonné[1]

Received 12 February 2013; revised 21 March 2013; accepted 21 March 2013; published 9 May 2013.

[1] Recently, it has been shown that the ionosphere is capable of showing images of seismic fault shortly after an earthquake. This gives rise to the idea of retrieval of seismic information from ionospheric observations. As the first step toward such inversion, here we study distinctive features of ionospheric response to shallow earthquakes, both submarine and inland, of moment magnitudes *Mw*7.2–9.1. Using GPS measurements of the ionospheric total electron content, we show that: (1) the amplitude of coseismic total electron content variations in the near-field is larger after more powerful earthquakes, and (2) stronger earthquakes ($M > 7.9$) are in general characterized by a longer negative phase in coseismic perturbations. **Citation:** Astafyeva, E., S. Shalimov, E. Olshanskaya, and P. Lognonné (2013), Ionospheric response to earthquakes of different magnitudes: Larger quakes perturb the ionosphere stronger and longer, *Geophys. Res. Lett.*, *40*, 1675–1681, doi:10.1002/grl.50398.

1. Introduction

[2] Earthquakes are known to be a source of atmospheric and ionospheric perturbations. During an earthquake, a sudden impulsive forcing from the ground generates atmospheric pressure waves that propagate upward into the atmosphere and ionosphere. They reach the *F* layer height of the ionosphere in 10 min or so. Due to the rapid decrease in atmospheric density with altitude, the corresponding velocities can attain rather large amplitudes. Resulting nonlinear effects lead to a shock formation represented by an N shaped waveform (Figure 1a) [e.g., *Zel'dovich and Raizer*, 1966]. Such N-type waveform is the response of the medium to a large amplitude impulsive forcing in which the compression, or positive phase, is followed by the "recovery" of the medium, the rarefaction, or negative phase [e.g., *Landau and Lifshitz*, 1995].

[3] Recently, propagation and spatio-temporal features of coseismic ionospheric disturbances (CID) have been extensively discussed in the scientific literature [e.g., *Calais and Minster*, 1995; *Heki and Ping*, 2005; *Astafyeva et al*., 2009; *Rolland et al*., 2011]. All these investigations confirm in general the N-shaped response of the ionosphere upon the shock-like atmospheric waves excited by coseismic vertical movements of the ground or the sea surface.

[4] The March 2011 earthquake in Japan has revealed the existence of at least four different types of coseismic perturbations in the ionosphere: those by propagating Rayleigh surface waves, those by the coseismic crustal displacements, those by tsunamis and postseismic 4 min monoperiodic atmospheric resonances [*Liu et al*., 2011; *Rolland et al*., 2011]. More recently, based on analysis of TEC response to the three largest submarine earthquakes in Japan, Chile, and Indonesia, *Kakinami et al*. [2012] have reported observations of a new type of CID, a sudden depletion of the ionospheric total electron content (TEC) that followed a sudden coseismic TEC enhancement and lasted afterward for a few tens of minutes. Because it was observed just *above* the tsunami source area, the ionospheric depletion was attributed "to the downwelling of the sea surface" due to the tsunami generation. *Kakinami et al*. [2012] also emphasize that inland earthquakes do not produce the ionospheric hole.

[5] Here we show that such kind of depletion rather represents the negative phase of the N-type response, whose duration depends on the magnitude of coseismic crustal vertical displacement. For this purpose, we study distinctive features of ionospheric response to shallow earthquakes of different magnitudes. It should be noted that oceanic earthquakes are often much more powerful than inland ones. The largest inland earthquake for the last decade, the Sichuan earthquake of 12 May 2008, was estimated to be 7.9 in magnitude, while the largest submarine events in Sumatra 2004 and in Japan 2011 were reported as $\sim M$ 9.0–9.1. Therefore, it is rather difficult to make a fully fledged comparative analysis of coseismic TEC variations initiated by both, inland and submarine earthquakes. Nevertheless, here we make a comparative analysis of features of submarine shallow earthquakes with moment magnitudes *Mw* 7.2–9.1.

2. Shallow Submarine Earthquakes

[6] General information on the analyzed events is shown in Table 1. Recently, it has been reported that ionospheric effects may depend on the focal mechanism of an earthquake [*Astafyeva and Heki*, 2009; *Gokhberg et al*., 2011]. Therefore, in this paper, to find the distinctions in coseismic features of earthquakes with different magnitudes, we have only analyzed events that can be characterized as reverse fault (thrust). The selected events are characterized as shallow earthquakes, with the depth of their hypocenter from 12 to 55 km.

[7] Earthquake #1 with magnitude 7.2, also known as Kii-earthquake or Kii-foreshock, occurred on 5 September 2004 at 10:07UT near the Kii Peninsula of Japan. A local tsunami was generated with wave heights of about 0.6 m in Kozushima [*Satake et al*., 2005].

Additional supporting information may be found in the online version of this article.

[1]Institut de Physique du Globe de Paris, Paris Sorbonne Cité, Univ. Paris Diderot, UMR 7154 CNRS, 75013, Paris, France.
[2]Institute of Physics of the Earth RAS, 123995, Moscow, Russia.
[3]Space Research Institute RAS, 117997, Moscow, Russia.

Corresponding author: E. Astafyeva, Institut de Physique du Globe de Paris, Paris Sorbonne Cité, Univ. Paris Diderot, UMR 7154 CNRS, Paris, France. (astafyeva@ipgp.fr)

0094-8276/13/10.1002/grl.50398

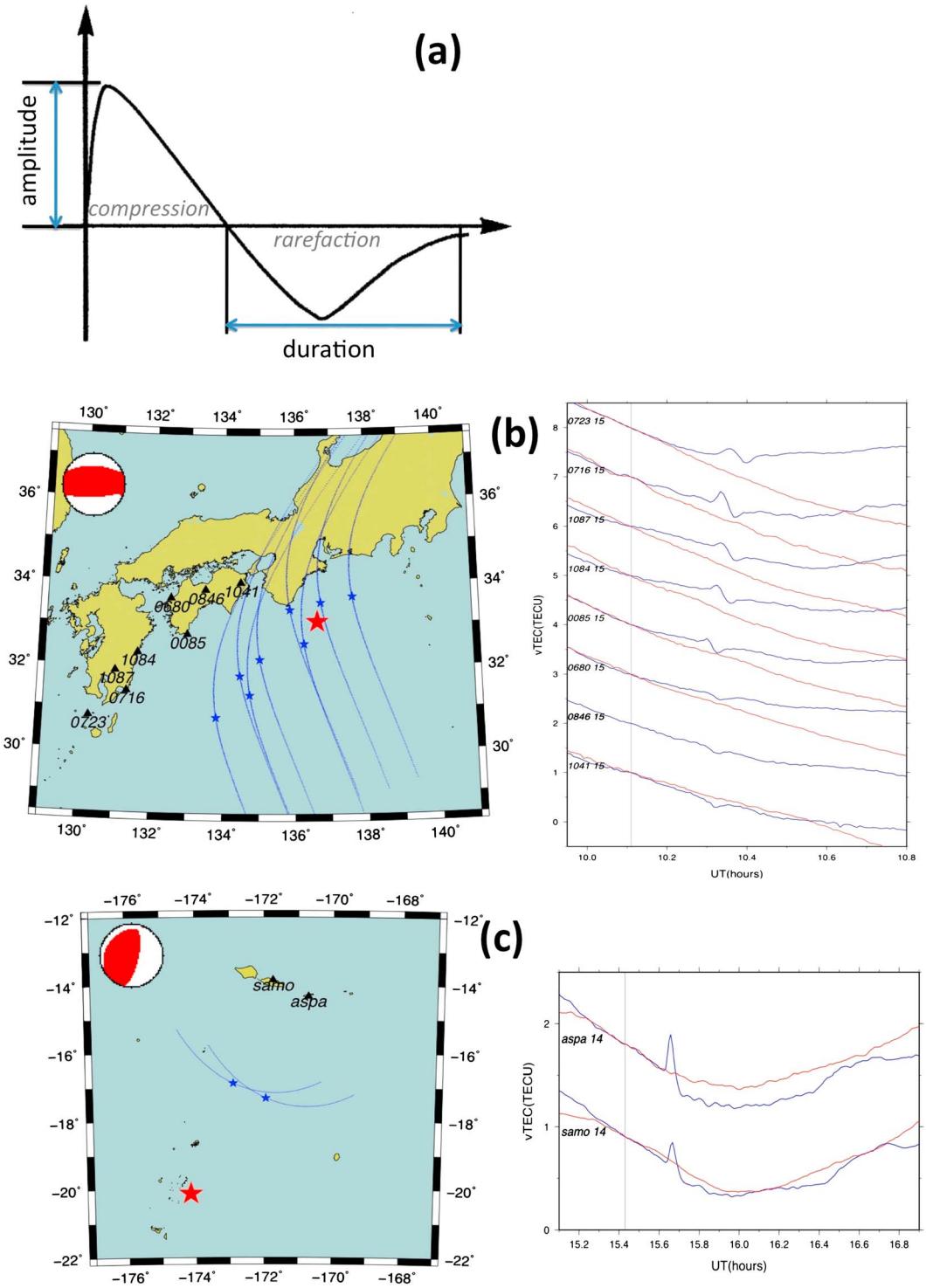

Figure 1. (a) Typical waveform of CID, N-wave. (b, c) Geometry of measurements (on the left) and coseismic TEC variations (on the right) for shallow submarine earthquakes: Kii earthquake of 4 September 2004 (Figure 1b); Tonga earthquake of 3 May 2006 (Figure 1c). Red star represents the epicenter, triangles show positions of GPS receivers, names of receivers are indicated next to the triangles, blue lines correspond to trajectories of ionospheric piercing points for certain satellites, small blue stars show position of IPP during the time of earthquake. To indicate the focal mechanism of the earthquake, the left panels show the "beach-balls." Panels on the right show variations of TEC measured by the GPS receivers on the day on earthquake (blue) and on reference day (red). Thin vertical gray line shows the moment of earthquakes. Name of a receiver and number of satellites are depicted on the panels.

Table 1. Information on Earthquakes (Date, Time, Location, Depth, Magnitude, Coseismic Crustal Uplift) and Parameters of TEC Response (Amplitude of VTEC and Duration of Negative Phase)

	Date	UT	Location (lat;lon)	*D*, Km	*Mw*	Vert. Disp, m	Amp, TECU	Duration, min
#1	2004/09/05	10:07:07	33.1; 136.6	14	7.2	0.42	0.2–0.3	4-8
#2	2006/05/03	15:26:39	–20.13;–174.16	55	7.9	1.22	0.35–0.5	40
#3	2009/07/15	09:22:29	–45.75; 166.58	12	7.8	0.95	0.28–0.4	5–6
#4	2011/03/09	02:45:20	38.44; 142.84	32	7.3	0.64	0.2–0.3	<4
#5	2011/03/11	05:46:24	38.3; 142.37	32	9.0	14.54	1.2–3	30–50
#6	1994/10/04	13:23:28	43.60; 147.63	61	8.1	0.84	0.4–0.7	20–40
#7	1999/09/20	17:47:35	23.87; 120.75	21	7.6	1.15	0.25	5–6
#8	2003/09/25	19:50:06	41.78; 143.90	28	8.3	1.95	0.5–0.7	20
#9	2004/12/26	00:58:53	3.32; 95.85	30	9.1	8.56	1.67	~30
10	2008/05/12	06:28:01	30.99; 103.36	13	7.9	2.89	0.6–1.2	~20
11	2010/02/27	06:34:14	35.91; 72.73	23	8.8	9.58	1.1–1.8	~20

[8] Earthquake #2 with moment magnitude 7.9 occurred on 3 May 2006 in the Tonga segment of the Tonga-Kermandec Subduction Zone, near the islands of the Kingdom of Tonga (http://earthquake.usgs.gov). A small tsunami with amplitude about 0.6 m was recorded by ocean buoys (http://www.drgeorgepc.com/Tsunami2006Tonga.html).

[9] Earthquake #3 with moment magnitude 7.8 struck the South Island of New Zealand at 9:22 UT on 15 July 2009. The earthquake generated a tsunami with maximum height of 0.47 m (http://tsunami.gov).

[10] Earthquake #4 occurred 2 days before the great Tohoku mega-thrust earthquake off the east coast of Japan, and it is known as a foreshock of the Tohoku earthquake. According to the USGS, the foreshock occurred at 02:45 UT. Its moment magnitude was estimated 7.3. The quake generated a small tsunami of maximum wave height of 0.6 m (http://www.jma.go.jp/en/tsunami/observation_04_20110309150337.html).

[11] Earthquake #5 is the well-known Tohoku mega-thrust earthquake that occurred on 11 March 2011 at 05:46:26 UT off the east coast of Honshu, Japan. Its moment magnitude was estimated 9.0. Five minutes in duration, the earthquake generated a huge tsunami with maximum height of 38 m in Ofunato region of Japan (Japanese Meteorological Agency, http://jma.go.jp).

3. Observations

[12] To study ionospheric response to the selected earthquakes, we use GPS measurements of ionospheric TEC derived from data of ground-based GPS receivers. For events that occurred in Japan, we processed data of the Japanese network GEONET; coseismic variations after the Tonga earthquake were analyzed by use of International GNSS Service (IGS) data. Ionospheric signatures of earthquake #3 were analyzed by use of the regional network of GPS receivers installed in New Zealand (http://geonet.org.nz).

[13] The technique to calculate the TEC from data of dual-frequency GPS receivers has been well described in detail in numerous papers [e.g., *Calais and Minster*, 1995; *Afraimovich et al*., 2001]. Because TEC is an integral parameter, it is impossible to determine the exact height of occurrence of an ionospheric perturbation. However, the main contribution to TEC variations appears around the height of the ionosphere maximum ionization. This allows us to consider the ionosphere as a thin layer located at the height h_{max} of the ionospheric F2 layer. TEC then represents a point of intersection of a line of sight with this thin layer, making it possible to track the propagation of ionospheric perturbations by subionospheric point (SIP), a projection of an ionospheric piercing point (IPP) to the Earth's surface. In this paper we assumed h_{max} to be at 250 km.

[14] Low elevation angles tend to enlarge the horizontal extent of the ionospheric region represented by one measurement, enlarging the sphericity effects. Therefore, we converted the slant TEC to vertical TEC by using the known Klobuchar's formula [*Klobuchar*, 1986]. Furthermore, here we adopt the same method as was used by *Kakinami et al*. [2012], i.e., we do not apply high-pass filtering so that we can see the long-lasting variations. To better understand the coseismic changes in TEC variations, we compare the data with the TEC of a reference day. However, we point out that the estimation of the duration of the negative phase essentially depends on the definition of the reference line. Here, following *Kakinami et al*. [2012], as a reference TEC we plot TEC for a geomagnetically quiet day. Although at each period of day a GPS satellite passes close to the region of a day before, the day-to-day ionospheric variability often plays the decisive role in value of TEC.

[15] It should be noted that the waveform and the amplitude of TEC response to earthquake significantly depend on the geometry of line of sight and on parameters of magnetic field (inclination and declination). Besides, the amplitude of TEC perturbations increases upon their equatorward propagation and reaches the maximum at ~500 km from the epicenter and further decreases with distance [*Astafyeva et al*., 2009]. In connection with that, in the present work, we analyze and compare amplitude of TEC variations registered over the epicenter and in the near-field of the earthquakes' epicenters (within ~ 400 km).

[16] Geometry of GPS measurements during the Kii-earthquake and TEC response to the quake are shown in Figure 1b. Even if the SIP of the closest GPS receivers and satellite 15 are located within 200 km from the epicenter, the amplitude and waveform of TEC variations essentially differ from receiver to receiver. For example, GPS stations 1041, 0846, 0680 located northward from the epicenter, show small-amplitude and hardly discernible perturbation ~12 min after the quake, while southwestern stations (1084, 0716, 1087, 0723) detected an N-shaped perturbation with amplitude 0.2–0.3 TECU (TEC units, 10^{16} electrons/m^2). Such "directivity" effect is caused by the geomagnetic field, which prohibits northward and northeastward propagation of ionospheric perturbations in the Northern Hemisphere [e.g., *Heki and Ping*, 2005]. The duration of the N wave negative phase is 4–5 min.

[17] Earthquakes #2 and #3 occurred in the Southern Hemisphere, so that we expect to observe northward propagation of

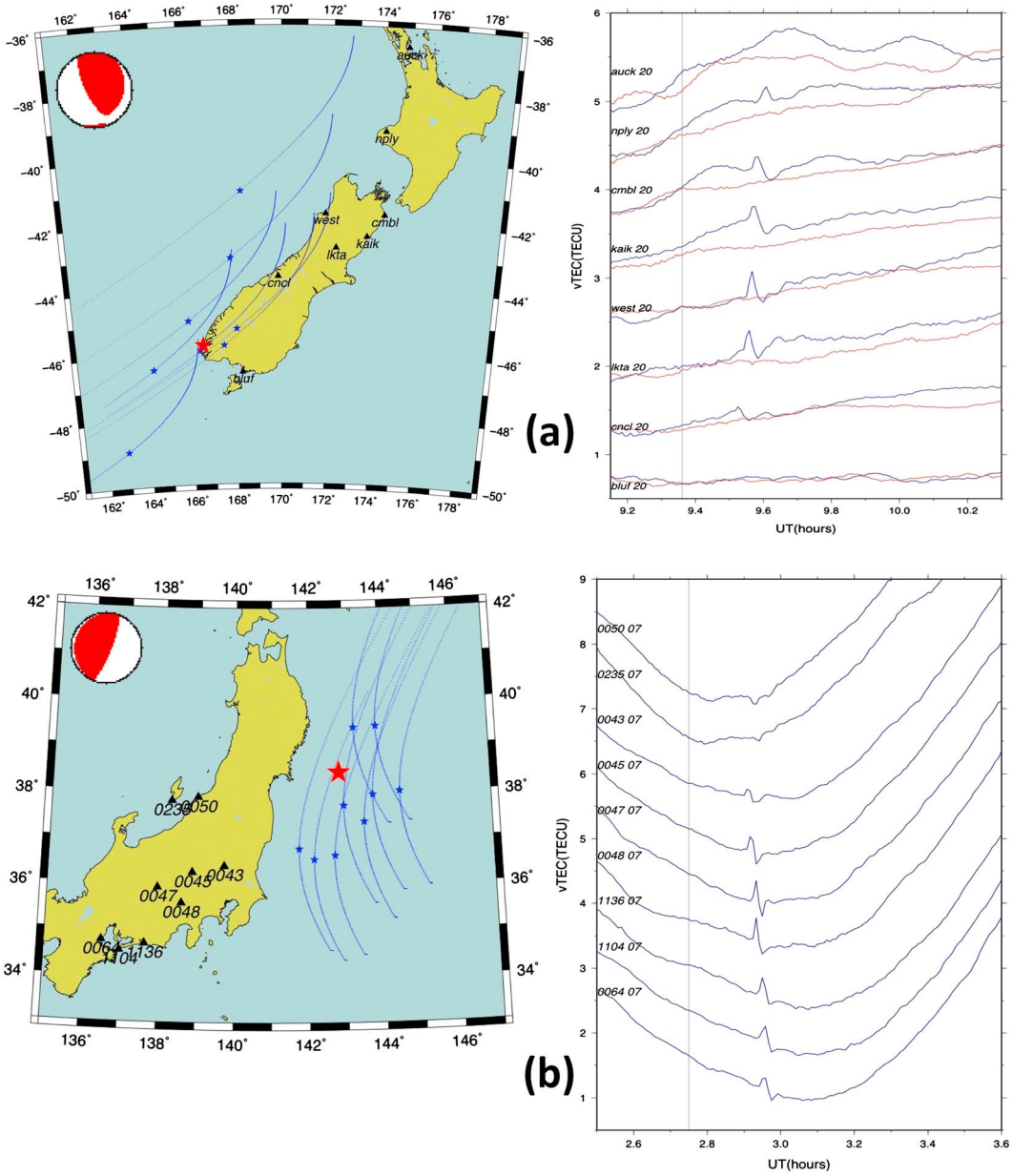

Figure 2. The same as Figures 1b and 1c but for (a) the New Zealand earthquake of 15 July 2009 and (b) the Tohoku foreshock of 9 March 2011.

CID and fast damping of perturbations in southward direction. Indeed, in case of the Tonga earthquake, the SIP of GPS receivers SAMO and ASPA were located ~360–390 km on the north-northeast from the epicenter. TEC response to the earthquake was detected by satellite PRN14 (Figure 1c). First arrival of TEC perturbation was registered 11–12 min after the quake, the amplitude of perturbation was registered to be 0.35–0.5 TECU, and the duration of the N wave negative phase is about 40 min.

[18] Coseismic perturbations generated by earthquake #3 were registered by GPS receivers of the New Zealand GPS-network and by satellite PRN 20 (Figure 2a). There was no perturbation detected at the southernmost station BLUF, because during the earthquake the IPP were located ~440 km on the south from the epicenter, which means propagation of CID in the direction opposite to the magnetic field. Small-amplitude response was observed at station CNCL, the small amplitude is also due to the influence of geomagnetic field. The nearest to the epicenter station LKTA showed N-shaped TEC variations as a response to this *M*7.8 earthquake. Other GPS stations detected similar N-responses. We did not observe coseismic signature at GPS receiver AUCK whose IPP were at 550–600 km away from the epicenter. It is known that the quake-generated perturbation fade out at such distances [*Astafyeva et al*, 2009]. The amplitude of the perturbation in the near-field of the source is 0.25–0.35 TECU, the duration of the N-wave negative phase is 5–6 min.

[19] Total electron content response to earthquake #4, the *M*7.3 Tohoku foreshock, is shown in Figure 2b. We do not observe any discernible TEC signatures at northernmost stations 0050 and 0235. Other receivers from Figure 2b show small-amplitude N-shaped TEC response to the earthquake. The first arrival was registered by GPS receiver

0045 at 2.91UT (9.6 min after the quake), and several minutes later the CID reached stations 0043 and 0047. The amplitude of the near-field TEC response is 0.2–0.3 TECU and the duration of the negative phase is less than 4 min.

[20] The coseismic perturbations generated by the 11 March 2011 Tohoku-oki earthquake have been discussed in detail in numerous papers [e.g., *Liu et al*., 2011; *Rolland et al*., 2011; *Astafyeva et al*., 2011; *Kakinami et al*., 2012]. Therefore, here we do not show the TEC data series, but only refer to previous papers. The near-field TEC-response was at best registered by GPS satellite 26, and overall the signal was quite superposed [*Astafyeva et al*., 2011]. The near-field peak-to-peak amplitude was estimated to be ~1–3 TECU, the duration of negative phase was ~40 min [*Kakinami et al*., 2012].

[21] We summarize the obtained results in Table 1. From the Table and Figures 1, 2 the following tendency follows: stronger earthquakes cause larger TEC perturbations. Besides, TEC response to stronger earthquakes (M>7.9) is characterized in general by a longer negative phase in coseismic perturbations.

4. Discussion

[22] Using GPS TEC measurements, we have analyzed TEC response to shallow earthquakes with magnitudes of M7.2–M9.1. In all cases, the waveform of the coseismic perturbation is N-wave, with the only difference in amplitude of the positive phase and duration of its negative phase. The N-wave is so named for its letter N-like shape, an initial overpressure half-cycle with a relatively fast risetime and a slower pressure decay followed by a half-cycle of rarefaction (Figure 1a). The N-wave consists, therefore, of regions of high/compression and low/rarefaction pressure (or corresponding velocities of alternating polarity). The Earth's atmosphere is a viscous medium with a decreasing density. When an atmospheric compression-rarefaction wave propagates upward through the inhomogeneous atmosphere, the wave amplitude increases so that the wave transforms into a shock-acoustic wave (or N-wave) due to nonlinear effects [e.g., *Zel'dovich and Raizer*, 1966].

[23] When a shock-acoustic wave reaches the upper ionosphere, the geomagnetic field inclination must be taken into account. Because the plasma there can move only along the magnetic field lines, the acoustic wave propagating southward and northward relative to the epicenter can make the plasma migrate upward and downward in different ways. This results in the so-called directivity effect and complicates the interpretation of alternating phases of signals observed in the ionosphere northward from epicenter (in the Northern Hemisphere). For example, sometimes only negative phase of the N-wave propagating with acoustic speed in the upper ionosphere can be seen on the north from the epicenter in Northern Hemisphere [e.g., *Heki and Ping*, 2005; *Gokhberg et al*., 2011]. Same sort of the effect can be also seen in our data.

[24] The phases of N-wave can get different duration [*Whitham*, 1974; *Naugolnikh and Ostrovsky*, 1998]. To explore this fact we refer to a simple explanation which can be found, for example, in the textbook by *Zel'dovich, and Raizer* [1966]. Specifically, for a compression shock wave (positive phase) propagating through the undisturbed gas at supersonic speed, the state behind the wave front can in no way affect the state of the gas ahead of the wave and the discontinuity remains stable. The significance of the formation of a negative phase is that essentially no more energy can reach the shock front from the source region. This results in relatively small deviation from the atmospheric pressure during negative phase. Therefore, to satisfy the requirement of zero algebraic sum of the areas occupied by both phases, the duration of the negative phase must be longer than the positive one. In other words, it follows that the larger the amplitude of the positive phase of a wave (which is determined in its turn by the uplift, see below), the longer can be its negative phase.

[25] In addition to that, it should be pointed out that a majority of powerful submarine earthquakes do generate tsunamis; however, the final height of tsunami waves would depend on a variety of parameters, including barometry, earthquakes' depth, and the amplitude of coseismic vertical displacements. The latter serves as a main source of ionospheric perturbations, while moment magnitude is an energetical parameter. Therefore, it is of interest to analyze the correlation between the coseismic crustal vertical displacement and the amplitude of CID.

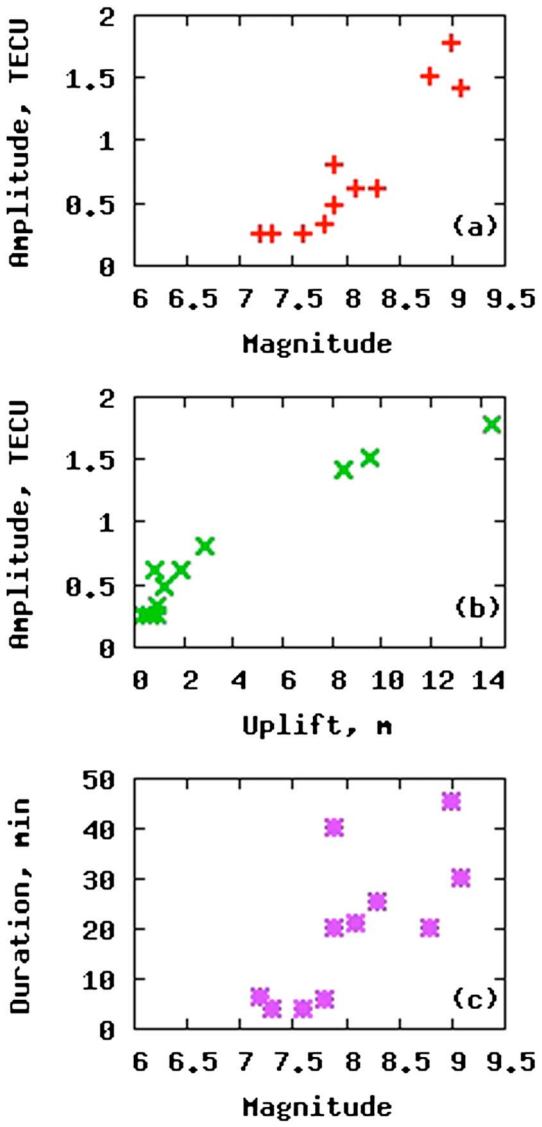

Figure 3. Amplitude of TEC perturbations versus magnitude of earthquakes (a) and coseismic uplift (b). (c) Duration of the negative phase of TEC response versus magnitude.

[26] Despite the complexity of seismic source and of the internal structure of the Earth, a relatively simple model for the source can be used to calculate coseismic vertical displacement [*Okada*, 1985]. Specifically, for a finite rectangular fault with length L and width W occurring at depth d, the surface deformation field due to shear and tensile faults in a half-space can be evaluated analytically. Rupture parameters (sizes, orientation, depth) can be determined from the Global CMT catalog (www.globalcmt.org). General dislocation can be determined by three angles: the dip angle δ of the fault, the slip angle θ, and the angle φ between the fault plane and Burger's vector D module of which is the displacement along the fault. Using this information, for each earthquake the fault plane can be chosen. The fault length L and width W were calculated using semiempirical formulas of *Kanamori and Anderson* [1975], *Riznichenko* [1992]:

$$\log L = 0.440Mw - 1.289$$

$$\log W = 0.401Mw - 1.448$$

[27] The displacement along the fault was calculated using formulas by *Chinnery* [1963]

$$\log D = 0.757Mw - 3.235$$

[28] Furthermore, using the information about the fault and the Poisson coefficient of the medium, and under assumption that the total work of elasticity force is transformed into the shear along the fault, the components of vector of coseismic surface deformation according to *Okada* [1985] can be calculated. The results of our calculations are presented in Table 1.

[29] To reinforce our statistics, here we present also parameters of TEC perturbations generated by some other large earthquakes (Table 1, lines #6–#11, and Figure S1), including two inland events: the M7.6 Chi-Chi earthquake in Taiwan, and M7.9 Sichuan earthquake of 12 May 2008 in China. Using the data from Table 1, we plot dependence of amplitude of TEC response on magnitude of an earthquake and on coseismic uplift (Figures 3a and 3b). It is obvious that quakes with larger magnitudes generate TEC perturbations of larger amplitudes. We note, however, that the amplitude of CID depends also on the geometry of GPS sounding and on the angle between the magnetic field vector and the perturbation wave vector; therefore, there can always exist an ambiguity in amplitude estimation.

[30] Dependence of duration of the negative phase on earthquake's magnitude is not as unambiguous as in the case of the amplitude (Figure 3c). One can see general tendency of "lengthening" of the negative phase with a magnitude. However, after some quakes with $M > 7.9$ the depletion can last from 20 to 40–50 min, i.e., the duration of the negative phase can vary significantly. In some cases the requirement of zero algebraic sum of the areas occupied by both phases is not exactly satisfied because of apparently long negative phase. We attribute this with imperfect conditions of observations and/or processes that need further in-depth study. In addition, we underline the method adopted in the present study. Following *Kakinami et al*. [2012], we do not apply high-pass filtering to the original data to make a comparison with their results. However, for example, the day-to-day ionospheric variability often plays the decisive role in TEC data series. Exclusion of such variability makes the dependence even more clear. The result of such procedure for the event 2006/05/03 can be seen in Figure S2 (auxiliary material).

[31] Using our results and the above discussion we suggest an alternative interpretation of the "tsunamigenic ionospheric hole" observed by *Kakinami et al*. [2012] after three large submarine earthquakes: in Japan (11 March 2011, M9.0), in Chile (27 February 2010, M8.8) and in Indonesia (26 December 2004, M9.1). They reported observation of a sudden TEC enhancement followed by a sudden depletion of the ionospheric TEC lasting for a few tens of minutes, and noted that "the large-scale depletion is located only over the tsunami source area and does not propagate." Regarding the mechanism producing the "hole" they claimed that "only the initial downwelling of tsunami produces the ionospheric hole and the propagation of tsunami does not produce it." As a consequence, they emphasized that "inland large EQs do not produce the ionospheric hole."

[32] According to our interpretation, the "hole" represents the negative phase of an N-wave. Our conclusion is supported by the spatial distribution of the depletion: it always appears at the same area as the positive perturbation, but ~10–15 min later. In addition, it is impossible for the initial downwelling of tsunami to produce any ionospheric hole, because it is known that such kind of source generates acoustic-gravity waves in which case acoustic waves transform into N waves in the ionosphere while gravity waves cannot propagate vertically upward, and it takes a few hours for them to reach the upper ionosphere. Besides, same sort of "ionospheric hole" has been observed after the Tohoku earthquake in data over South Korea, which is ~1000 km from the seismic source and where no coseismic crustal subsidence occurred (Figure S1d). Therefore, the observed depletion is hardly related to the occurrence of the tsunami, but rather related to the magnitude of a quake, either submarine or inland.

5. Conclusions

[33] The present study demonstrates that stronger earthquakes (whether inland or submarine) generate TEC perturbations of larger amplitude with longer negative phases that can be seen as long-lasting ionospheric depletions. Shallow earthquakes with magnitude M7.2–7.8 cause coseismic perturbations with near-field amplitude of 0.2–0.4 TECU, while mega-earthquakes of ~M9.0 produce extremely large perturbations of ~1–3 TECU in amplitude. In the same manner, the duration of negative phase of coseismic perturbations generated by a M7.2–7.8 earthquake is from 4 to 8 min, whereas by M9.0 earthquake—about 30–40 min. We expect that further works would make it possible to estimate parameters of seismic source from ionospheric data like in *Astafyeva et al*. [2011], and our work is only a first step toward this goal. To make such inversions possible, further observations and especially modeling are necessary, but it is out of the scope of the present paper.

[34] **Acknowledgments.** This work was initiated under the support of the French National Research Agency ("To_EOS" Project ANR-11-JAPN-008), and was finalized under the support of the European Research Council under the European Union's Seventh Framework Program/ERC grant agreement 307998. We thank the Geospatial Information Authority of Japan for the data of the GPS Earth Observation Network System (GEONET), the SOPAC archive for IGS GPS data and the official source of geological hazard information for New Zealand for data of GPS receivers installed in New Zealand. We thank B.-K. Choi (Korea Astronomy and Space Science Institute) for data of Korean GPS Network KGN. This is IPGP contribution 3392.

[35] The Editor thanks Kosuke Heki and Shingo Watada for their assistance in evaluating this paper.

References

Afraimovich, E. L., N. P. Perevalova, A. V. Plotnikov, and A. M. Uralov (2001), The shock-acoustic waves generated by the earthquakes, *Ann. Geophys.*, *19*(4), 395–409.

Astafyeva, E., K. Heki, V. Kiryushkin, E. L. Afraimovich, and S. Shalimov (2009), Two-mode long-distance propagation of coseismic ionosphere disturbances, *J. Geophys. Res.*, V. *114*, A10307, doi:10.1029/2008JA013853.

Astafyeva, E., and K. Heki (2009), Dependence of waveform of near-field coseismic ionospheric disturbances on focal mechanisms, *Earth. Planet. Space*, *61*, 939–943.

Astafyeva, E., P. Lognonné, and L. Rolland (2011), First ionosphere images for the seismic slip of the Tohoku-oki earthquake, *Geophys. Res. Lett.*, *V.38*, L22104, doi:10.1029/2011GL049623.

Calais, E., and J. B. Minster (1995), GPS detection of ionospheric perturbations following the January 17, 1994, Northridge earthquake, *Geophys. Res. Lett.*, *22*, 1045–1048, doi:10.1029/95GL00168.

Chinnery, M. A. (1963), The stress changes that accompany strike-slip faulting, *Bull. Seism. Soc. Am.*, *53*, 921–932.

Gokhberg, M. B., V. M. Lapshin, G. M. Steblov, and S. L. Shalimov (2011), Ionospheric Response to Kuril Undersea Earthquakes According to GPS Satellite Data, *Izv. Atmos. Oceanic Phys.*, *47*(9), 1019–1027.

Heki, K., and J. Ping (2005), Directivity and apparent velocity of the coseismic ionospheric disturbances observed with a dense GPS array, *Earth Planet. Sci. Lett.*, *236*, 845–855, doi:10.1016/j.epsl.2005.06.010.

Kakinami, Y., M. Kamogawa, Y. Tanioka, S. Watanabe, A. R. Gusman, J.-Y. Liu, Y. Watanabe, and T. Mogi (2012), Tsunamigenic ionospheric hole, *Geophys. Res. Lett.*, *39*, L00G27, doi:10.1029/2011GL050159.

Kanamori, H., and D. Anderson (1975), Theoretical basis of some empirical ralations in seismology, *Bull. Seism. Soc. Am.*, *65*(5), 1073–1095.

Klobuchar, J. A. (1986), Ionospheric time-delay algorithm for single frequency GPS users, *IEEE Trans. on Aerosp. Electron. Syst., AES*, *23*(3), 325–331.

Landau, L. D., and E. M. Lifshitz (1995), Fluid Mechanics, *Course of Theoretical Physics* Vol. *6*, (1st edn.), Pergamon Press, ISBN 978-0-08-009104-4.

Liu, J.-Y., C.-H. Chen, C.-H. Lin, H.-F. Tsai, C.-H. Chen, and M. Kamogawa (2011), Ionospheric disturbances triggered by the 11 March 2011 *M*9.0 Tohoku earthquake, *J. Geophys. Res.*, *116*, A06319, doi:10.1029/2011JA016761.

Okada, Y. (1985), Surface deformation due shear tensile faults half space, *Bull. Seism. Soc. Am.*, *75*(4), 1135–1154.

Naugolnikh, K., Ostrovsky L. (1998), *Non-linear wave processes in acoustics*, 312p, Cambridge University Press, IBSN 978-0521399845.

Riznichenko, Yu. V. (1992), *Problems of seismology*, 445 p, Springer-Verlag, ISBN: 978-0387542300.

Rolland, L., P. Lognonne, E. Astafyeva, A. Kherani, N. Kobayashi, M. Mann, and H. Munekane (2011), The resonant response of the ionosphere imaged after the 2011 Tohoku-Oki earthquake, *Earth. Planet. Space*, *63*(7), doi:10.5047/eps.2011.06.020.

Satake, K., T. Baba, K. Hirata, S. Iwasaki, T. Kato, S. Koshimura, J. Takenaka, and Y. Terada (2005), Tsunami source of the 2004 off the Kii Peninsula earthquakes inferred from offshore tsunami and coastal tide gauges, *Earth Planet. Space*, *57*, 173–178.

Whitham, G. B. (1974), *Linear and Nonlinear waves*, J. Wiley & Sons, NY, 622 pp.

Zel'dovich, Ya. B., and Yu. P. Raizer (1966), *Physics of Shock Waves and High-Temperature Hydrodynamic Phenomena*, V.*1*, 464pp, Academic Press, NY & London.